PADOVA UNIVERSITY PRESS

Dolomites Research Notes on Approximation

Special Issue for the "10 years of the Padua points", Volume 8 · 2015 · Pages 23–36

A survey on bivariate Lagrange interpolation on Lissajous nodes

Wolfgang Erb[a] · Christian Kaethner[b] · Peter Dencker[a] · Mandy Ahlborg[b]

Abstract

This article is a survey on recent research on bivariate polynomial interpolation on the node points of Lissajous curves. The resulting theory is a generalization of the generating curve approach developed for Lagrange interpolation on the Padua points. After classifying the different types of Lissajous curves, we give a short overview on interpolation and quadrature rules defined on the node points of the Lissajous curves. Further, we summarize some convergence results and show how the interpolating polynomials can be computed efficiently. Finally, the developed theory is applied to a practical problem from a medical imaging modality called Magnetic Particle Imaging.

1 Introduction

In 2005, the Padua points were introduced in [9] as a new and promising set of node points for bivariate polynomial interpolation. A major issue in high order polynomial interpolation is its ill-conditioning, in particular if the underlying set of interpolation nodes is unfavourably chosen. In this regard, the Padua points turn out to be distributed advantageously in $[-1,1]^2$. A result in [3] states that for the Padua points the absolute condition of the interpolation problem grows only logarithmically in the number of interpolation nodes.

Beside their favourable behavior in terms of stability, the Padua points have some more outstanding properties. They allow unique polynomial interpolation in the space Π^N of bivariate polynomials of degree N, they can be characterized as an affine variety of a polynomial ideal [5] and they form a particular Chebyshev lattice of rank 1 [12]. Moreover, the interpolating polynomial can be computed in an efficient way by using fast Fourier methods [8, 10]. Particularly interesting for the aim of this article is the fact that the Padua points can also be described as the node points of particular degenerate Lissajous curves [3].

In a novel medical imaging modality called Magnetic Particle Imaging (MPI), the data acquisition path of the scanning device is typically given by a Lissajous curve [26, 38]. In order to obtain a bivariate polynomial interpolation of data values on these curves, extensions of the generating curve approach of the Padua points were studied in [15, 16]. Thereby, not all mentioned properties of the Padua points can be carried over to the larger framework of Lissajous figures. However, the resulting theory on interpolation and quadrature based on the node points of Lissajous curves has strong resemblances to the respective theory of the Padua points. Moreover, there are also relations to other well-known point sets as the Morrow-Patterson points [30], the Xu points [39] and some generalizations of these node sets [24].

The goal of this article is to give a compact survey on recent research about polynomial interpolation on Lissajous curves. The presented results are mainly taken from [15, 16] and are linked to well-known results of the Padua points, the Xu points or the theory of polynomial reconstruction on Chebyshev lattices [12, 32, 34]. As an application of the presented theory, we review a practical problem from MPI related to data acquisition on elongated Lissajous curves [25].

This survey article is organized as follows. In Section 2, we give a short introduction to Lissajous curves and the properties of their node points. In Section 3 and 4, we develop quadrature rules and an interpolation theory based on the node points of the Lissajous curves. Then, in Section 5 we give a short overview on convergence and stability of the interpolating schemes. Afterwards, the efficient computation of the interpolating polynomial is discussed in Section 6. In the final Section 7, we investigate a practical problem related to Lissajous trajectories in MPI.

2 Characterization of Lissajous curves

From a physical point of view, a Lissajous curve describes the path of a double pendulum in the plane that moves with two different frequencies n_1 and n_2 in orthogonal directions. If n_1 and n_2 are integers, the resulting curve is closed and it can be parametrized mathematically by

$$\gamma^{(\underline{n})}_{\underline{\kappa},\underline{u}} : [0,2\pi] \to [-1,1]^2, \quad \gamma^{(\underline{n})}_{\underline{\kappa},\underline{u}}(t) := \begin{pmatrix} u_1 \cos(n_2 t - \kappa_1 \pi/(2n_1)) \\ u_2 \cos(n_1 t - \kappa_2 \pi/(2n_2)) \end{pmatrix}$$

with $\underline{n} = (n_1, n_2) \in \mathbb{N}^2$ and $\underline{\kappa} = (\kappa_1, \kappa_2) \in \mathbb{R}^2$, $\underline{u} \in \{-1,1\}^2$.

Lissajous curves and their properties are studied since the early 19th century. They are named after the french physician Joseph A. Lissajous who showed their physical significance in an extensive treatise [28]. A classical reference for the mathematical characterization of two-dimensional Lissajous curves and its singularities is the dissertation of Braun [6]. In recent years, Lissajous

[a] Institute of Mathematics, Universität zu Lübeck, Ratzeburger Allee 160, 23562 Lübeck
[b] Institute of Medical Engineering, Universität zu Lübeck, Ratzeburger Allee 160, 23562 Lübeck

curves have been studied mainly in terms of knot theory, see [1, 27]. Relations between degenerate Lissajous curves and Chebyshev curves are described in [17, 27].

In the following, we assume that the natural numbers n_1 and n_2 are relatively prime. Under this condition, 2π is the minimal period of $\Upsilon^{(\underline{n})}_{\underline{\kappa},\underline{u}}$. The curve $\Upsilon^{(\underline{n})}_{\underline{\kappa},\underline{u}}$ is called degenerate if $\kappa_2-\kappa_1\in 2\mathbb{Z}$ and non-degenerate otherwise. This definition is easily seen to be independent of the parameter $\underline{u}$. In the following, we will see that the geometric properties of degenerate and non-degenerate Lissajous curves differ considerably. In particular, the terminology degenerate descends from the fact that a degenerate curve $\Upsilon^{(\underline{n})}_{\underline{\kappa},\underline{u}}$ is doubly traversed as t varies from 0 to 2π.

Proposition 2.1. *There exist $t'\in\mathbb{R}$, $\eta\in[0,2)$ and $\underline{u}'\in\{-1,1\}^2$ such that*

$$\Upsilon^{(\underline{n})}_{\underline{\kappa},\underline{u}}(t-t')=\Upsilon^{(\underline{n})}_{(0,\eta),\underline{u}'}(t),\quad t\in[0,2\pi]. \tag{1}$$

The curve $\Upsilon^{(\underline{n})}_{\underline{\kappa},\underline{u}}$ is degenerate if and only if $\eta=0$ in (1). Further, if $\underline{\kappa}\in\mathbb{Z}^2$, the value of η can always be chosen from $\{0,1\}$.

Proof. Obviously, we find a t'' such that $\Upsilon^{(\underline{n})}_{\underline{\kappa},\underline{u}}(t-t'')=\Upsilon^{(\underline{n})}_{\underline{\kappa}',\underline{u}}(t)$ with $\kappa_1'=0$. Let a be the unique integer with $0\le a+\kappa_2'/2<1$. Since n_1 and n_2 are relatively prime, we can find two integers $k,l\in\mathbb{Z}$ such that $a=kn_1+ln_2$. Let $t'=t''+k\pi/n_2$, $\eta=2a+\kappa_2'$. Now, since

$$n_1(t-t')-\kappa_2\pi/(2n_2)=n_1(t-k\pi/n_2)-\kappa_2'\pi/(2n_2)=n_1t-\eta\pi/(2n_2)+l\pi,\quad n_2(t-t')-\kappa_1\pi/(2n_1)=n_2t-k\pi,$$

we obtain (1) for $u_1'=(-1)^k u_1$ and $u_2'=(-1)^l u_2$. The curve $\Upsilon^{(\underline{n})}_{\underline{\kappa},\underline{u}}$ is degenerate if and only if $\Upsilon^{(\underline{n})}_{(0,\eta),\underline{u}'}$ is degenerate. Since $\eta\in[0,2)$, the property $\eta\in2\mathbb{Z}$ is valid if and only if $\eta=0$. For the last statement, note that $\underline{\kappa}\in\mathbb{Z}^2$ implies $\kappa_2'\in\mathbb{Z}$ and therefore that η is an integer in $[0,2)$. □

Many Lissajous curves that are important in applications have integer-valued parameters $\underline{\kappa}\in\mathbb{Z}^2$. As seen in Proposition 2.1, such curves can be written in the form (1) with $\eta\in\{0,1\}$ differing only in the reflection parameter $\underline{u}'$. We will therefore restrict our considerations to the curves

$$\gamma^{(\underline{n})}_\epsilon:[0,2\pi]\to[-1,1]^2,\quad \gamma^{(\underline{n})}_\epsilon(t):=\Upsilon^{(\underline{n})}_{(0,\epsilon-1),\underline{1}}(t)=\begin{pmatrix}\cos(n_2t)\\ \cos\left(n_1t+(\epsilon-1)\pi/(2n_2)\right)\end{pmatrix} \tag{2}$$

with a parameter $\epsilon\in\{1,2\}$ and the fixed reflection parameter $\underline{1}=(1,1)$. In particular, up to a shift t' and up to reflections with respect to the coordinate axis, all degenerate curves can be written in the form $\gamma^{(\underline{n})}_1$. In the same way, all curves with $\underline{\kappa}\in\mathbb{Z}^2$ which are non-degenerate, i.e. $\kappa_2-\kappa_1$ is odd, can be transformed to the curve $\gamma^{(\underline{n})}_2$.

Example 2.1. (i) The generating curves of the Padua points are the degenerate curves $\Upsilon^{(n,n+1)}_{\underline{0},\underline{u}}$ or $\Upsilon^{(n+1,n)}_{\underline{0},\underline{u}}$, $n\in\mathbb{N}$, see [3]. Up to the reflection parameter $\underline{u}$, they can be written in the form $\gamma^{(n,n+1)}_1$ or $\gamma^{(n+1,n)}_1$.

(ii) In [15], the generating curve approach of the Padua points was extended to general degenerate curves of the form

$$\gamma^{(n+p,n)}_1(t)=\begin{pmatrix}\cos(nt)\\ \cos((n+p)t)\end{pmatrix},$$

with relatively prime natural numbers n and p.

(iii) In [16], Lissajous curves of the form

$$\Upsilon^{(n+p,n)}_{(n+p,n),\underline{1}}(t)=\begin{pmatrix}\sin(nt)\\ \sin((n+p)t)\end{pmatrix},\quad n,p\in\mathbb{N}, \tag{3}$$

were used as generating curves for bivariate interpolation. Again, n and p are assumed to be relatively prime. If p is odd, Proposition 2.1 states that this curve can be rewritten in the non-degenerate form $\gamma^{(n+p,n)}_2$. If p is even, the situation is different. In this case not considered in [16], the curve (3) is degenerate and can be reformulated as $\gamma^{(n+p,n)}_1$.

Now, we draw our attention to sets of node points that are generated by the Lissajous curves $\gamma^{(\underline{n})}_\epsilon$, $\epsilon\in\{1,2\}$. For this, we define the equidistant time samples

$$t^{(\epsilon\underline{n})}_k:=\frac{\pi k}{\epsilon n_1n_2},\quad k=0,\dots,2\epsilon n_1n_2-1,$$

and introduce the following sets of Lissajous node points:

$$\mathrm{LS}^{(\underline{n})}_\epsilon:=\left\{\gamma^{(\underline{n})}_\epsilon(t^{(\epsilon\underline{n})}_k):\quad k=0,\dots,2\epsilon n_1n_2-1\right\}. \tag{4}$$

Note that in the non-degenerate case the shift $t'\in\mathbb{R}$ in Proposition (2.1) can be chosen in such a way that the set $\mathrm{LS}^{(\underline{n})}_2$ remains invariant if we substitute $\gamma^{(\underline{n})}_2$ in (4) by an arbitrary non-degenerate curve $\Upsilon^{(\underline{n})}_{\underline{\kappa},\underline{u}}$ with $\underline{\kappa}\in\mathbb{Z}^2$. Therefore, the set $\mathrm{LS}^{(n+p,n)}_2$ is exactly the set of node points considered in [16].

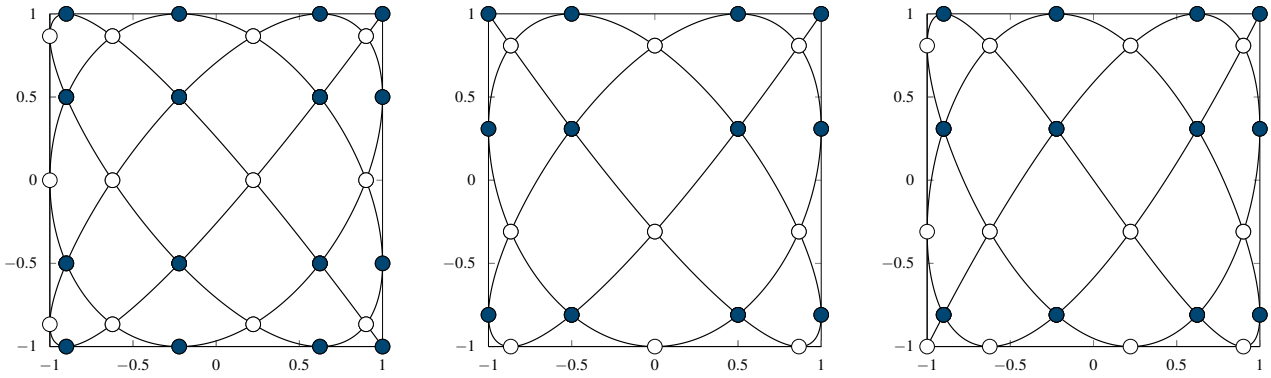

(a) $\gamma_1^{(7,6)}$, $\#\mathrm{LS}_1^{(7,6)} = 28$. (b) $\gamma_1^{(6,5)}$, $\#\mathrm{LS}_1^{(6,5)} = 21$. (c) $\gamma_1^{(7,5)}$, $\#\mathrm{LS}_1^{(7,5)} = 24$.

Figure 1: Illustration of degenerate Lissajous curves $\gamma_1^{(\boldsymbol{n})}$ and its node points $\mathrm{LS}_1^{(\boldsymbol{n})}$ according to the cases in Table 1. The points in the subgrids $\mathrm{LS}_{\mathrm{b},1}^{(\boldsymbol{n})}$ and $\mathrm{LS}_{\mathrm{w},1}^{(\boldsymbol{n})}$ are colored in blue and white, respectively.

Number of node points		
$\#\mathrm{LS}_1^{(\boldsymbol{n})} = \frac{(n_1+1)(n_2+1)}{2}$	$\#\mathrm{LS}_{\mathrm{int},1}^{(\boldsymbol{n})} = \frac{(n_1-1)(n_2-1)}{2}$	$\#\mathrm{LS}_{\mathrm{out},1}^{(\boldsymbol{n})} = n_1+n_2$

Case (a): n_1 odd, n_2 even	Case (b): n_1 even, n_2 odd	Case (c): n_1 odd, n_2 odd
$\#\mathrm{LS}_{\mathrm{b},1}^{(\boldsymbol{n})} = \frac{n_1+1}{2}\frac{n_2+2}{2}$	$\#\mathrm{LS}_{\mathrm{b},1}^{(\boldsymbol{n})} = \frac{n_1+2}{2}\frac{n_2+1}{2}$	$\#\mathrm{LS}_{\mathrm{b},1}^{(\boldsymbol{n})} = \frac{n_1+1}{2}\frac{n_2+1}{2}$
$\#\mathrm{LS}_{\mathrm{w},1}^{(\boldsymbol{n})} = \frac{n_1+1}{2}\frac{n_2}{2}$	$\#\mathrm{LS}_{\mathrm{w},1}^{(\boldsymbol{n})} = \frac{n_1}{2}\frac{n_2+1}{2}$	$\#\mathrm{LS}_{\mathrm{w},1}^{(\boldsymbol{n})} = \frac{n_1+1}{2}\frac{n_2+1}{2}$
$\gamma_1^{(\boldsymbol{n})}(\pi) = (1,-1)$	$\gamma_1^{(\boldsymbol{n})}(\pi) = (-1,1)$	$\gamma_1^{(\boldsymbol{n})}(\pi) = (-1,-1)$

Table 1: Number of node points in the different subsets of $\mathrm{LS}_1^{(\boldsymbol{n})}$.

2.1 Degenerate Lissajous curves

For a degenerate Lissajous curve $\gamma_1^{(\boldsymbol{n})}$, we have $\gamma_1^{(\boldsymbol{n})}(t) = \gamma_1^{(\boldsymbol{n})}(2\pi - t)$ for all $t \in [0, 2\pi]$. Therefore, $\gamma_1^{(\boldsymbol{n})}$ is traversed twice as t runs from 0 to 2π and it is sufficient to restrict the parametrization of $\gamma_1^{(\boldsymbol{n})}$ to the interval $[0,\pi]$. Further, the points $\gamma_1^{(\boldsymbol{n})}(0)$ and $\gamma_1^{(\boldsymbol{n})}(\pi)$ are located at the edges $(1,1)$ and $((-1)^{n_2},(-1)^{n_1})$ of the square $[-1,1]^2$. Three examples of degenerate curves $\gamma_1^{(\boldsymbol{n})}$ are illustrated in Figure 1.

We start to investigate the self-intersection points of the curve $\gamma_1^{(\boldsymbol{n})}$. Two values $t \neq t'$ describing the same point $\gamma_1^{(\boldsymbol{n})}(t) = \gamma_1^{(\boldsymbol{n})}(t')$ satisfy the equations

$$0 = \cos(n_i t) - \cos(n_i t') = -2\sin\left(n_i \frac{t+t'}{2}\right)\sin\left(n_i \frac{t-t'}{2}\right), \quad i \in \{1,2\}.$$

This is the case if t and t' satisfy

$$\text{(i)} \quad t + t' = 2j\pi/n_2 \quad \text{or} \quad \text{(i)}' \quad t - t' = 2j\pi/n_2 \quad \text{for} \quad j \in \mathbb{Z},$$

and

$$\text{(ii)} \quad t + t' = 2i\pi/n_1 \quad \text{or} \quad \text{(ii)}' \quad t - t' = 2i\pi/n_1 \quad \text{for} \quad i \in \mathbb{Z}.$$

Since n_1 and n_2 are relatively prime the conditions (i) and (ii) as well as (i)′ and (ii)′ can not be combined if we assume that $t \neq t'$ and $t, t' \in [0,\pi]$. Therefore, combining (i) with (ii)′ and (i)′ with (ii), we obtain

$$t = \left(\frac{i}{n_1} + \frac{j}{n_2}\right)\pi, \quad t' = \pm\left(\frac{i}{n_1} - \frac{j}{n_2}\right)\pi, \quad i,j \in \mathbb{Z}, \tag{5}$$

as a necessary condition for $\gamma_1^{(\boldsymbol{n})}(t)$ to be a self-intersection point. This implies that every self-intersection point is included in the node set $\mathrm{LS}_1^{(\boldsymbol{n})}$.

Since n_1 and n_2 are relatively prime, every $k \in \mathbb{Z}$ can be written as $k = in_2 + jn_1$ with $i,j \in \mathbb{Z}$. If we define the index set

$$\Gamma^{(\boldsymbol{n})} := \left\{(i,j) \in \mathbb{N}_0^2 : \frac{i}{n_1} + \frac{j}{n_2} < 1\right\} \cup \{(0,n_2)\}, \tag{6}$$

we obtain

$$\mathrm{LS}_1^{(\underline{n})} = \Big\{\gamma_1^{(\underline{n})}(t_k^{(\underline{n})}) : \quad k \in \mathbb{Z}\Big\} = \Big\{\gamma_1^{(\underline{n})}\Big(\frac{in_2 + jn_1}{n_1 n_2}\pi\Big) : \quad (i,j) \in \mathbb{Z}^2\Big\} = \Big\{\gamma_1^{(\underline{n})}\Big(\frac{in_2 + jn_1}{n_1 n_2}\pi\Big) : \quad (i,j) \in \Gamma^{(\underline{n})}\Big\}. \tag{7}$$

By (5) and the definition (6) of the index set $\Gamma^{(\underline{n})}$, all points on the right hand side of (7) are distinct for different (i,j). Since n_1 and n_2 are relatively prime we can immediately get the size of the index set $\Gamma^{(\underline{n})}$ and thus the size of $\mathrm{LS}_1^{(\underline{n})}$ as

$$\#\mathrm{LS}_1^{(\underline{n})} = \#\Gamma^{(\underline{n})} = \frac{(n_1+1)(n_2+1)}{2}.$$

Finally, we determine the actual intersection points in $\mathrm{LS}_1^{(\underline{n})}$. To this end we consider again the necessary condition (5). In (5), we have $t = t'$ if and only if $i = 0$ or $j = 0$. For all other points we have $t \neq t'$, and therefore, a self-intersection point of the curve $\gamma_1^{(\underline{n})}$. The points $\gamma_1^{(\underline{n})}(t_{in_2+jn_1}^{(\underline{n})})$ with $i = 0$ or $j = 0$ are located on the boundary of the domain $[-1,1]^2$. Thus, the node set $\mathrm{LS}_1^{(\underline{n})}$ is the disjoint union of the set $\mathrm{LS}_{\mathrm{int},1}^{(\underline{n})}$ of self-intersection points and a set $\mathrm{LS}_{\mathrm{out},1}^{(\underline{n})}$ of boundary points of the Lissajous curve $\gamma_1^{(\underline{n})}$. They are explicitly given as

$$\mathrm{LS}_{\mathrm{int},1}^{(\underline{n})} := \Big\{\gamma_1^{(\underline{n})}(t_{in_2+jn_1}^{(\underline{n})}) : \quad (i,j) \in \Gamma^{(\underline{n})},\ i,j \neq 0\Big\}$$

and

$$\mathrm{LS}_{\mathrm{out},1}^{(\underline{n})} := \Big\{\gamma_1^{(\underline{n})}(t_{in_2+jn_1}^{(\underline{n})}) : \quad (i,j) \in \Gamma^{(\underline{n})},\ i = 0 \text{ or } j = 0\Big\}.$$

Further, we observe in Figure 1 that the set $\mathrm{LS}_1^{(\underline{n})}$ is a disjoint union of two grids $\mathrm{LS}_{\mathrm{b},1}^{(\underline{n})}$ and $\mathrm{LS}_{\mathrm{w},1}^{(\underline{n})}$. From the upcoming characterization (11) and (12) of the points as Chebyshev-Gauß-Lobatto points, the number of points in the different subsets can be computed explicitly. They are listed in Table 1. Moreover, exactly two points of the degenerate Lissajous curves $\gamma_1^{(\underline{n})}$ are located in the corners of the square $[-1,1]^2$. They are given as

$$\mathrm{LS}_{\mathrm{vert},1}^{(\underline{n})} := \Big\{\gamma_1^{(\underline{n})}(0), \gamma_1^{(\underline{n})}(\pi)\Big\} = \{(1,1), ((-1)^{n_2}, (-1)^{n_1})\}.$$

2.2 Non-degenerate Lissajous curves

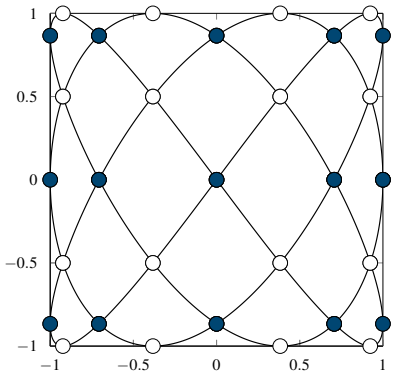

(a) $\gamma_2^{(4,3)}$, $\#\mathrm{LS}_2^{(4,3)} = 31$.

Number of node points
$\#\mathrm{LS}_2^{(\underline{n})} = 2n_1n_2 + n_1 + n_2$
$\#\mathrm{LS}_{\mathrm{int},2}^{(\underline{n})} = 2n_1n_2 - n_1 - n_2$
$\#\mathrm{LS}_{\mathrm{out},2}^{(\underline{n})} = 2n_1 + 2n_2$
$\#\mathrm{LS}_{\mathrm{b},2}^{(\underline{n})} = (n_1+1)n_2$
$\#\mathrm{LS}_{\mathrm{w},2}^{(\underline{n})} = n_1(n_2+1)$

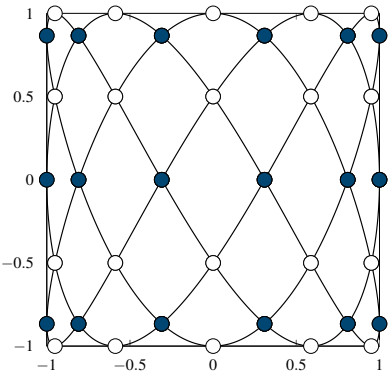

(b) $\gamma_2^{(5,3)}$, $\#\mathrm{LS}_2^{(5,3)} = 38$.

Figure 2: Illustration of two non-degenerate Lissajous curves $\gamma_2^{(\underline{n})}$ with the respective node points $\mathrm{LS}_2^{(\underline{n})}$. In the center, the cardinalities of the different subsets of $\mathrm{LS}_2^{(\underline{n})}$ are listed.

For a non-degenerate curve $\gamma_2^{(\underline{n})}$, the conditions on t, t' to describe a self-intersection point of $\gamma_2^{(\underline{n})}$ look slightly different than in (5). For $t \neq t'$ with $\gamma_2^{(\underline{n})}(t) = \gamma_2^{(\underline{n})}(t')$ it is necessary that (see [1])

$$t = \left(\frac{i}{n_1} + \frac{j}{n_2}\right)\pi, \quad t' = \left(-\frac{i}{n_1} + \frac{j}{n_2}\right)\pi, \quad i,j \in \mathbb{Z}, \tag{8}$$

or

$$t = \left(\frac{i}{n_1} + \frac{j}{n_2} - \frac{1}{2n_1n_2}\right)\pi, \quad t' = \left(\frac{i}{n_1} - \frac{j}{n_2} - \frac{1}{2n_1n_2}\right)\pi, \quad i,j \in \mathbb{Z}. \tag{9}$$

As in the degenerate case, the conditions (8) or (9) imply that all self-intersection points $\mathrm{LS}_{\mathrm{int},2}^{(\underline{n})}$ are included in $\mathrm{LS}_2^{(\underline{n})}$. Moreover, we obtain a natural disjoint decomposition of $\mathrm{LS}_2^{(\underline{n})}$ in the two sets

$$\mathrm{LS}_{\mathrm{b},2}^{(\underline{n})} := \Big\{\gamma_2^{(\underline{n})}(t_{2k}^{(2\underline{n})}) : \quad k = 0, \dots, 2n_1n_2 - 1\Big\},$$
$$\mathrm{LS}_{\mathrm{w},2}^{(\underline{n})} := \Big\{\gamma_2^{(\underline{n})}(t_{2k-1}^{(2\underline{n})}) : \quad k = 1, \dots, 2n_1n_2\Big\}.$$

In view of (8), the value t generates a self-intersection point in $\mathrm{LS}_{\mathrm{b},2}^{(\underline{n})}$ if and only if $i \notin n_1\mathbb{Z}$. Therefore, we have $2n_2$ elements in $\mathrm{LS}_{\mathrm{b},2}^{(\underline{n})}$ that are not self-intersection points and that lie on the boundary of $[-1,1]^2$. In the same way, we obtain $2n_1$ elements of $\mathrm{LS}_{\mathrm{w},2}^{(\underline{n})}$ on the boundary of $[-1,1]^2$. In total, the set $\mathrm{LS}_{\mathrm{out},2}^{(\underline{n})} \subset \mathrm{LS}_2^{(\underline{n})}$ of node points lying on the boundary of $[-1,1]^2$ consists of $2n_1+2n_2$ points. Therefore we can compute the number of self-intersection points of the curve $\gamma_2^{(\underline{n})}$ as

$$\#\mathrm{LS}_{\mathrm{int},2}^{(\underline{n})} = \frac{4n_1n_2 - 2n_1 - 2n_2}{2} = 2n_1n_2 - n_1 - n_2.$$

This implies in particular that the number of elements in $\mathrm{LS}_2^{(\underline{n})}$ is given by

$$\#\mathrm{LS}_2^{(\underline{n})} = \#\mathrm{LS}_{\mathrm{int},2}^{(\underline{n})} + \#\mathrm{LS}_{\mathrm{out},2}^{(\underline{n})} = 2n_1n_2 + n_1 + n_2.$$

Two examples of the node sets $\mathrm{LS}_2^{(\underline{n})}$ and the cardinalities of the different subsets are illustrated in Figure 2. Similar as the index set (6) in the case of degenerate curves, the set

$$\Gamma^{(2\underline{n})} = \Gamma^{(2n_1,2n_2)} = \left\{(i,j) \in \mathbb{N}_0^2 : \ \frac{i}{2n_1} + \frac{j}{2n_2} < 1\right\} \cup \{(0,2n_2)\}, \tag{10}$$

plays an important role for bivariate polynomial interpolation in the non-degenerate case. However, in the non-degenerate case a direct relation to the Lissajous nodes as given in (7) is not known. Nevertheless, a simple geometric argument shows that

$$\#\Gamma^{(2\underline{n})} = \frac{(2n_1+1)(2n_2+1)-1}{2} = 2n_1n_2 + n_1 + n_2 = \#\mathrm{LS}_2^{(\underline{n})}.$$

Two examples of different index sets $\Gamma^{(\epsilon\underline{n})}$ are illustrated in Figure 3.

In contrast to the degenerate case, the point set $\mathrm{LS}_2^{(\underline{n})}$ is symmetric with respect to reflections at the coordinate axis. Furthermore, there are no points of $\mathrm{LS}_2^{(\underline{n})}$ on the vertices of the square $[-1,1]^2$, i.e. $\mathrm{LS}_{\mathrm{vert},2}^{(\underline{n})} = \emptyset$. This can easily be seen from the representation of the sets $\mathrm{LS}_\epsilon^{(\underline{n})}$ with Chebyshev-Gauß-Lobatto points given in the next section.

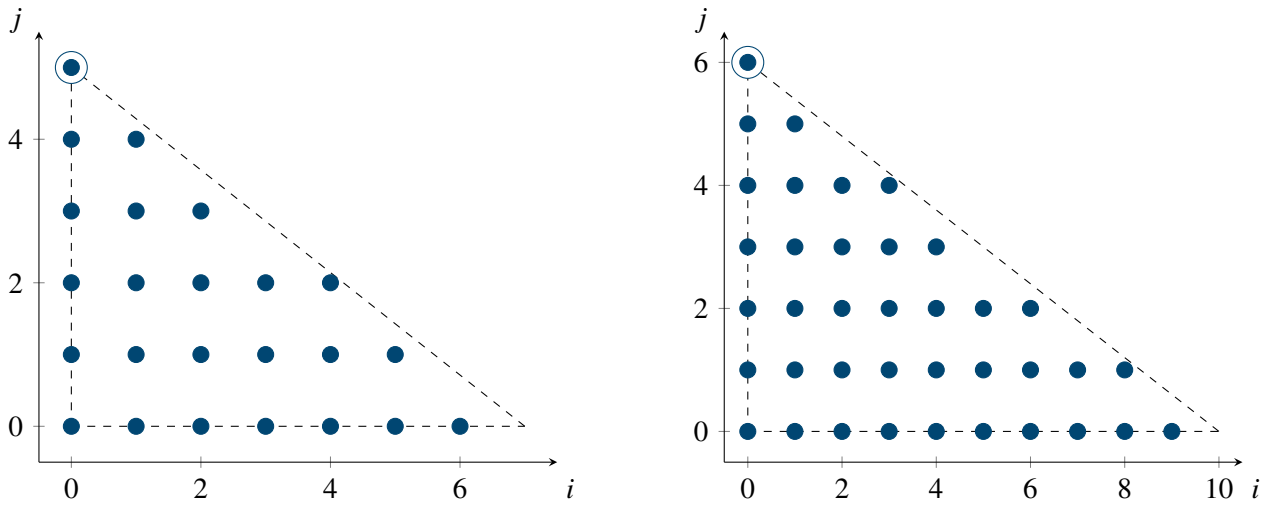

(a) Index set $\Gamma^{(7,5)}$, $\#\Gamma^{(7,5)} = \#\mathrm{LS}_1^{(7,5)} = 24$.

(b) Index set $\Gamma^{(10,6)}$, $\#\Gamma^{(10,6)} = \#\mathrm{LS}_2^{(5,3)} = 38$.

Figure 3: Illustration of two index sets $\Gamma^{(\epsilon\underline{n})}$ corresponding to the Lissajous node points $\mathrm{LS}_\epsilon^{(\underline{n})}$. The sets $\Gamma^{(\epsilon\underline{n})}$ are contained in the marked simplices $\{(x,y) \in \mathbb{R} : \ x \geq 0, \ y \geq 0, \ x/n_1 + y/n_2 \leq \epsilon\}$. The point $(0, \epsilon n_2)$ is the only element of $\Gamma^{(\epsilon\underline{n})}$ lying on the line $x/n_1 + y/n_2 = \epsilon$.

2.3 Characterization of the sets $\mathrm{LS}_\epsilon^{(\underline{n})}$ with Chebyshev-Gauß-Lobatto points

The node points of the Chebyshev-Gauß-Lobatto quadrature rule on the interval $[-1,1]$ are given as

$$z_k^n := \cos\left(\frac{k\pi}{n}\right), \quad n \in \mathbb{N}, \ k = 0, \dots, n.$$

Using this notation, the node sets $\mathrm{LS}_\epsilon^{(\underline{n})}$ can be compactly characterized as

$$\mathrm{LS}_\epsilon^{(\underline{n})} = \left\{ \left(z_r^{\epsilon n_1}, z_s^{\epsilon n_2}\right) : \begin{array}{l} r = 0, \dots, \epsilon n_1 \\ s = 0, \dots, \epsilon n_2 \\ r + s = \epsilon - 1 \mod 2 \end{array} \right\}. \tag{11}$$

To derive (11) a few simple manipulations of the defining equation (2) are necessary. The single derivations can be found in [15] for the degenerate case and in [16] for the non-degenerate case. Using the characterization (11), the self-intersection and the boundary points of $\mathrm{LS}_\epsilon^{(\underline{n})}$ can be written explicitly as

$$\mathrm{LS}_{\mathrm{int},\epsilon}^{(\underline{n})} = \left\{ \left(z_r^{\epsilon n_1}, z_s^{\epsilon n_2}\right) : \begin{array}{l} r = 1,\dots,\epsilon n_1 - 1 \\ s = 1,\dots,\epsilon n_2 - 1 \\ r+s = \epsilon - 1 \mod 2 \end{array} \right\}$$

and

$$\mathrm{LS}_{\mathrm{out},\epsilon}^{(\underline{n})} = \left\{ \left(z_r^{\epsilon n_1}, z_s^{\epsilon n_2}\right) : \begin{array}{ll} r = 0,\dots,\epsilon n_1, & s \in \{0, \epsilon n_2\} \\ r \in \{0, \epsilon n_1\}, & s = 0,\dots,\epsilon n_2 \\ r+s = \epsilon - 1 \mod 2 & \end{array} \quad \text{or} \right\}.$$

Further, in (11) we can directly see that $\mathrm{LS}_\epsilon^{(\underline{n})}$ is a disjoint union of two rectangular grids. These grids are given as

$$\mathrm{LS}_{\mathrm{b},\epsilon}^{(\underline{n})} = \left\{ \left(z_r^{\epsilon n_1}, z_s^{\epsilon n_2}\right) : \begin{array}{l} r = 0,\dots,\epsilon n_1 \\ s = 0,\dots,\epsilon n_2 \\ r = 0 \mod 2 \\ s = \epsilon - 1 \mod 2 \end{array} \right\}, \quad \mathrm{LS}_{\mathrm{w},\epsilon}^{(\underline{n})} = \left\{ \left(z_r^{\epsilon n_1}, z_s^{\epsilon n_2}\right) : \begin{array}{l} r = 0,\dots,\epsilon n_1 \\ s = 0,\dots,\epsilon n_2 \\ r = 1 \mod 2 \\ s = \epsilon \mod 2 \end{array} \right\}. \tag{12}$$

In Figure 1 and 2, the two grids are marked with blue and white dots, respectively.

3 Quadrature rules on Lissajous node points

The sets $\mathrm{LS}_\epsilon^{(\underline{n})}$ are interesting as node points for bivariate Lagrange interpolation as well as for quadrature rules with respect to a product Chebyshev weight. In this section, we will show that a large class of algebraic polynomials can be integrated exactly if we use $\mathrm{LS}_\epsilon^{(\underline{n})}$ as an underlying set of quadrature nodes. As polynomial spaces on $[-1,1]^2$, we consider

$$\Pi^N := \mathrm{span}\{T_i(x)T_j(y) : \ i + j \le N\},$$

where $T_i(x)$ denote the Chebyshev polynomials $T_i(x) = \cos(i \arccos x)$ of the first kind. It is well-known (cf. [14, 39]) that $\{T_i(x)T_j(y) : \ i+j \le N\}$ forms an orthogonal basis of the space Π^N with respect to the inner product

$$\langle f, g \rangle := \frac{1}{\pi^2} \int_{-1}^{1} \int_{-1}^{1} f(x,y) g(x,y) \omega(x,y) \mathrm{d}x\mathrm{d}y, \quad \omega(x,y) := \frac{1}{\sqrt{1-x^2}} \frac{1}{\sqrt{1-y^2}}. \tag{13}$$

The corresponding normalized basis can be also formulated explicitly as $\{\hat{T}_i(x)\hat{T}_j(y) : i+j \le N\}$, where

$$\hat{T}_i(x) := \begin{cases} 1, & \text{if } i = 0, \\ \sqrt{2} T_i(x), & \text{if } i \neq 0. \end{cases}$$

Finding suitable quadrature and interpolation nodes for the space Π^N is a challenging task on its own behalf. Among others, the Padua and the Xu points have been developed exactly for this purpose. However, for interpolation based on the Lissajous nodes $\mathrm{LS}_\epsilon^{(\underline{n})}$ other polynomial spaces reflecting the asymmetric structure of the points $\mathrm{LS}_\epsilon^{(\underline{n})}$ are more suited. We can define these polynomial with help of the index sets $\Gamma^{(\epsilon\underline{n})}$ given in (6) and (10). We set

$$\Pi^{(\epsilon\underline{n})} := \mathrm{span}\{T_i(x)T_j(y) : \ (i,j) \in \Gamma^{(\epsilon\underline{n})}\}, \quad \epsilon \in \{1,2\}, \tag{14}$$

and obtain immediately

$$\dim \Pi^{(\underline{n})} = \#\Gamma^{(\underline{n})} = \#\mathrm{LS}_1^{(\underline{n})}, \quad \dim \Pi^{(2\underline{n})} = \#\Gamma^{(2\underline{n})} = \#\mathrm{LS}_2^{(\underline{n})}.$$

Therefore, the polynomial spaces $\Pi^{(\epsilon\underline{n})}$, $\epsilon \in \{1,2\}$, are natural candidates as interpolation spaces for the sets $\mathrm{LS}_\epsilon^{(\underline{n})}$. On the other hand, for quadrature rules on $\mathrm{LS}_\epsilon^{(\underline{n})}$ the spaces $\Pi^{(2\epsilon\underline{n})}$ turn out to be interesting. They are defined as in (14) with ϵ replaced by 2ϵ. For the proof of the quadrature formula, the following Lemma is the central step. It states that for a large class of algebraic polynomials a double integral of the form (13) can be reduced to a one-dimensional integral along the Lissajous curve $\boldsymbol{\gamma}_\epsilon^{(\underline{n})}$.

Lemma 3.1. *For all bivariate polynomials P satisfying $\langle P, T_{\epsilon k n_1}(x) T_{\epsilon k n_2}(y) \rangle = 0$, $k \in \mathbb{N}$, the following identity holds:*

$$\frac{1}{\pi^2} \int_{-1}^{1} \int_{-1}^{1} P(x,y) \omega(x,y) \mathrm{d}x\mathrm{d}y = \frac{1}{2\pi} \int_0^{2\pi} P(\boldsymbol{\gamma}_\epsilon^{(\underline{n})}(t)) \mathrm{d}t. \tag{15}$$

Proof. One has to check equation (15) for all basis polynomials $T_i(x)T_j(y)$, $(i,j) \in \mathbb{N}_0^2$. On the left hand side of (15), we get the value 1 if $(i,j) = (0,0)$ and 0 otherwise. On the right hand side of (15), we get also 1 if $(i,j) = (0,0)$. For $(i,j) \neq (0,0)$, we get

for the basis polynomials $P(x,y) = T_i(x)T_j(y)$ the expression

$$\begin{aligned}\frac{1}{2\pi}\int_0^{2\pi} P(\boldsymbol{\gamma}_\epsilon^{(\underline{\boldsymbol{n}})}(t))\mathrm{d}t &= \frac{1}{2\pi}\int_0^{2\pi} T_i(\cos(n_2 t))T_j\left(\cos\left(n_1 t + \frac{\epsilon-1}{2n_2}\pi\right)\right)\mathrm{d}t \\ &= \frac{1}{2\pi}\int_0^{2\pi} \cos(in_2 t)\cos\left(jn_1 t + j\frac{\epsilon-1}{2n_2}\pi\right)\mathrm{d}t \\ &= \frac{1}{4\pi}\int_0^{2\pi} \cos\left((in_2 - jn_2)t - j\frac{\epsilon-1}{2n_2}\pi\right)\mathrm{d}t.\end{aligned}$$

This integral can differ from zero only if $in_2 = jn_1$. Since n_1 and n_2 are relatively prime, this is only be the case if $i = kn_1$, $j = kn_2$ and $k \in \mathbb{N}$. In the case $\epsilon = 1$ this is also a sufficient condition for the right hand side to be different from 0. In the case $\epsilon = 2$, the indices $j = (2k+1)n_2$, $k \in \mathbb{N}$ lead also to a vanishing right hand side. Thus, for $\epsilon = 2$, the integral on the right hand side vanishes if and only if $i = kn_1$, $j = kn_2$ and $k \in 2\mathbb{N}$. □

In the subsequent part, we will use the notation $\mathcal{A} = (x_\mathcal{A}, y_\mathcal{A})$ for points in the node set $\mathrm{LS}_\epsilon^{(\underline{\boldsymbol{n}})}$. To formulate the quadrature rule explicitly, we introduce the following weights for $\mathcal{A} \in \mathrm{LS}_\epsilon^{(\underline{\boldsymbol{n}})}$:

$$w_\mathcal{A} := \frac{1}{\epsilon^2 n_1 n_2} \cdot \begin{cases} 2, & \text{if } \mathcal{A} \in \mathrm{LS}_{\mathrm{int},\epsilon}^{(\underline{\boldsymbol{n}})}, \\ 1, & \text{if } \mathcal{A} \in \mathrm{LS}_{\mathrm{out},\epsilon}^{(\underline{\boldsymbol{n}})} \setminus \mathrm{LS}_{\mathrm{vert},\epsilon}^{(\underline{\boldsymbol{n}})}, \\ 1/2, & \text{if } \mathcal{A} \in \mathrm{LS}_{\mathrm{vert},\epsilon}^{(\underline{\boldsymbol{n}})}. \end{cases}$$

The case $\mathcal{A} \in \mathrm{LS}_{\mathrm{vert},\epsilon}^{(\underline{\boldsymbol{n}})}$ is only relevant in the degenerate case $\epsilon = 1$. We obtain the following quadrature rule:

Theorem 3.2. *For all polynomials $P \in \Pi^{(2\epsilon\underline{\boldsymbol{n}})}$ with $\langle P, T_{2\epsilon n_2}(y)\rangle = 0$, the quadrature formula*

$$\frac{1}{\pi^2}\int_{-1}^{1}\int_{-1}^{1} P(x,y)\omega(x,y)\mathrm{d}x\mathrm{d}y = \sum_{\mathcal{A}\in\mathrm{LS}_\epsilon^{(\underline{\boldsymbol{n}})}} w_\mathcal{A} P(\mathcal{A})$$

is exact. For the particular polynomial $P(x,y) = (\hat{T}_{\epsilon n_2}(y))^2$ we have

$$\frac{1}{\pi^2}\int_{-1}^{1}\int_{-1}^{1} |\hat{T}_{\epsilon n_2}(y)|^2\omega(x,y)\mathrm{d}x\mathrm{d}y = \frac{1}{2}\sum_{\mathcal{A}\in\mathrm{LS}_\epsilon^{(\underline{\boldsymbol{n}})}} w_\mathcal{A}|\hat{T}_{\epsilon n_2}(y_\mathcal{A})|^2 = 1.$$

Proof. For all trigonometric 2π-periodic polynomials q of degree less than $2\epsilon n_1 n_2$, the following composite trapezoidal quadrature rule is exact:

$$\frac{1}{2\pi}\int_0^{2\pi} q(t)\mathrm{d}t = \frac{1}{2\epsilon n_1 n_2}\sum_{k=1}^{2\epsilon n_1 n_2} q\left(t_k^{(\epsilon\underline{\boldsymbol{n}})}\right).$$

By Lemma 3.1, we have for $P \in \Pi^{(\epsilon\underline{\boldsymbol{n}})}$ the identity

$$\frac{1}{\pi^2}\int_{-1}^{1}\int_{-1}^{1} P(x,y)\omega(x,y)\mathrm{d}x\mathrm{d}y = \frac{1}{2\pi}\int_0^{2\pi} P(\boldsymbol{\gamma}_\epsilon^{(\underline{\boldsymbol{n}})}(t))\mathrm{d}t.$$

If $P \in \Pi^{(2\epsilon\underline{\boldsymbol{n}})}$ and $\langle P, T_{2\epsilon n_2}(y)\rangle$, then the trigonometric polynomial $P(\boldsymbol{\gamma}^{(\underline{\boldsymbol{n}})}(t))$ is of degree less than $2\epsilon n_1 n_2$ and we get the quadrature formula

$$\frac{1}{\pi^2}\int_{-1}^{1}\int_{-1}^{1} P(x,y)\omega(x,y)\mathrm{d}x\mathrm{d}y = \frac{1}{2\epsilon n_1 n_2}\sum_{k=1}^{2\epsilon n_1 n_2} P(\boldsymbol{\gamma}^{(\underline{\boldsymbol{n}})}(t_k^{(\epsilon\underline{\boldsymbol{n}})})) = \sum_{\mathcal{A}\in\mathrm{LS}_\epsilon^{(\underline{\boldsymbol{n}})}} w_\mathcal{A} P(\mathcal{A}).$$

For the last equality, we used the fact that self-intersection points (in contrast to points of $\mathrm{LS}_\epsilon^{(\underline{\boldsymbol{n}})}$ on the boundary of $[-1,1]^2$) are counted twice. Moreover, in the degenerate case, all points $t_k^{(\underline{\boldsymbol{n}})}$ (except $t_{2n_1n_2}^{(\underline{\boldsymbol{n}})} = 0$ and $t_{n_1n_2}^{(\underline{\boldsymbol{n}})} = \pi$) are traversed twice.

We show the last formula by a direct calculation. Clearly $\|\hat{T}_{\epsilon n_2}(y)\|^2 = \frac{2}{\pi}\int_0^\pi \cos^2(\epsilon n_2 t)\mathrm{d}t = 1$. On the other hand, we get

$$\sum_{\mathcal{A}\in\mathrm{LS}_\epsilon^{(\underline{\boldsymbol{n}})}} w_\mathcal{A}|\hat{T}_{\epsilon n_2}(y_\mathcal{A})|^2 = \frac{1}{2\epsilon n_1 n_2}\sum_{k=1}^{2\epsilon n_1 n_2} 2\cos^2\left(\epsilon n_1 n_2 t_k^{(\epsilon\underline{\boldsymbol{n}})} + (\epsilon-1)\pi\right) = \frac{1}{\epsilon n_1 n_2}\sum_{k=1}^{2\epsilon n_1 n_2}\cos^2((k+\epsilon-1)\pi) = 2.$$

□

Remark 1. The ideas for the proof of Lemma 3.1 and Theorem 3.2 were originally developed in the generating curve approach [3] of the Padua points. Similar quadrature formulas exist also for other bivariate quadrature nodes as the Morrow-Patterson points, the Xu points (see [23, 30, 39]) or the Geronimus nodes (see [24]). The general construction of multidimensional nodes for cubature and interpolation purposes is a far-reaching topic and has a long history. For an overview and further literature, we refer to the survey articles [11, 19, 18] and the book [14].

Remark 2. The node sets $\mathrm{LS}_\epsilon^{(\underline{n})}$ are related to another well-known approach for multidimensional quadrature and interpolation based on Chebyshev lattices [12, 32, 33, 34]. According to the notation given in [12, 33], the sets $\mathrm{LS}_\epsilon^{(\underline{n})}$ are two-dimensional Chebyshev lattices of rank 1 with parameters $d_1 = \epsilon n_1 n_2$, $\mathbf{z}_1 = [n_2, n_1]$ and $\mathbf{z}_\Delta / d_\Delta = [0, \frac{\epsilon-1}{2n_2}]$. For general Chebyshev lattices, interpolation can be shown only in an approximative way known as hyperinterpolation (see [36]). In the following section we will see that the particular node sets $\mathrm{LS}_\epsilon^{(\underline{n})}$ combined with the index sets $\Gamma^{(\epsilon\underline{n})}$ allow unique polynomial interpolation.

4 Interpolation on Lissajous node points

Now, considering $\mathcal{A} \in \mathrm{LS}_\epsilon^{(\underline{n})}$ as node points for bivariate interpolation with given data values $f(\mathcal{A}) \in \mathbb{R}$, we want to find an unique interpolating polynomial $\mathcal{L}_\epsilon^{(\underline{n})} f$ in $[-1,1]^2$ that satisfies

$$\mathcal{L}_\epsilon^{(\underline{n})} f(\mathcal{A}) = f(\mathcal{A}) \quad \text{for all } \mathcal{A} \in \mathrm{LS}_\epsilon^{(\underline{n})}. \tag{16}$$

In the bivariate setting, it is a priori not clear which polynomial space is best suited to obtain a solution $\mathcal{L}_\epsilon^{(\underline{n})} f$ of (16). However, since $\dim \Pi^{(\epsilon\underline{n})} = \#\mathrm{LS}_\epsilon^{(\underline{n})}$, a promising first choice is the polynomial space $\Pi^{(\epsilon\underline{n})}$. To describe the fundamental polynomials of Lagrange interpolation in this setup, we introduce the reproducing kernel $K^{(\epsilon\underline{n})} : \mathbb{R}^2 \times \mathbb{R}^2 \to \mathbb{R}$ of the polynomial spaces $\Pi^{(\epsilon\underline{n})}$ as

$$K^{(\epsilon\underline{n})}(x, y; x', y') := \sum_{(i,j) \in \Gamma^{(\epsilon\underline{n})}} \hat{T}_i(x) \hat{T}_i(x') \hat{T}_j(y) \hat{T}_j(y').$$

Then, for $\mathcal{A} \in \mathrm{LS}_\epsilon^{(\underline{n})}$, we define define the polynomials $L_\mathcal{A} \in \Pi^{(\epsilon\underline{n})}$ as

$$L_\mathcal{A}(x, y) = w_\mathcal{A} \left(K^{(\epsilon\underline{n})}(x, y; x_\mathcal{A}, y_\mathcal{A}) - \frac{1}{2} \hat{T}_{\epsilon n_2}(y) \hat{T}_{\epsilon n_2}(y_\mathcal{A}) \right), \quad \mathcal{A} = (x_\mathcal{A}, y_\mathcal{A}) \in \mathrm{LS}_\epsilon^{(\underline{n})}. \tag{17}$$

Theorem 4.1. *The interpolation problem* (16) *has the unique solution*

$$\mathcal{L}_\epsilon^{(\underline{n})} f(x, y) = \sum_{\mathcal{A} \in \mathrm{LS}_\epsilon^{(\underline{n})}} f(\mathcal{A}) L_\mathcal{A}(x, y)$$

in the polynomial space $\Pi^{(\epsilon\underline{n})}$.

The coefficients $c_{ij} = \langle \mathcal{L}_\epsilon^{(\underline{n})} f, \hat{T}_i(x) \hat{T}_j(y) \rangle$ *of* $\mathcal{L}_\epsilon^{(\underline{n})} f$ *with respect to the orthonormal Chebyshev basis* $\{\hat{T}_i(x)\hat{T}_j(y) : (i,j) \in \Gamma^{(\epsilon\underline{n})}\}$ *of* $\Pi^{(\epsilon\underline{n})}$ *can be computed as*

$$c_{ij} = \begin{cases} \displaystyle\sum_{\mathcal{A} \in \mathrm{LS}_\epsilon^{(\underline{n})}} w_\mathcal{A} f(\mathcal{A}) \hat{T}_i(x_\mathcal{A}) \hat{T}_j(y_\mathcal{A}), & \text{if } (i,j) \in \Gamma^{(\epsilon\underline{n})} \setminus (0, \epsilon n_2), \\ \displaystyle\frac{1}{2} \sum_{\mathcal{A} \in \mathrm{LS}_\epsilon^{(\underline{n})}} w_\mathcal{A} f(\mathcal{A}) \hat{T}_{\epsilon n_2}(y_\mathcal{A}), & \text{if } (i,j) = (0, \epsilon n_2). \end{cases} \tag{18}$$

Proof. In comparison to the proofs in [15, 16], we give a simple direct proof.

We denote the space of real functions on the set $\mathrm{LS}_\epsilon^{(\underline{n})}$ as $\mathbb{R}^{\mathrm{LS}_\epsilon^{(\underline{n})}}$. On the vector space $\mathbb{R}^{\mathrm{LS}_\epsilon^{(\underline{n})}}$, we define the inner product

$$\langle g, g' \rangle_w = \sum_{\mathcal{A} \in \mathrm{LS}_\epsilon^{(\underline{n})}} w_\mathcal{A} g(\mathcal{A}) g'(\mathcal{A}), \qquad g, g' \in \mathbb{R}^{\mathrm{LS}_\epsilon^{(\underline{n})}},$$

and consider the functions $e^{(i,j)} \in \mathbb{R}^{\mathrm{LS}_\epsilon^{(\underline{n})}}$ given by $e^{(i,j)}(\mathcal{A}) = \hat{T}_i(x_\mathcal{A}) \hat{T}_j(y_\mathcal{A})$. For the basis polynomials $\hat{T}_i(x)\hat{T}_j(y), \hat{T}_{i'}(x)\hat{T}_{j'}(y) \in \Pi^{(\epsilon\underline{n})}$ with $(i,j) \neq (i',j')$, we have the inequality $i/n_1 + j/n_2 + i'/n_1 + j'/n_2 < 2\epsilon$ and, thus, $\hat{T}_i(x)\hat{T}_j(y)\hat{T}_{i'}(x)\hat{T}_{j'}(y) \in \Pi^{(2\epsilon\underline{n})}$. Applying the quadrature rule of Theorem 3.2 to this product, we get for $(i,j) \neq (i',j')$:

$$\left\langle e^{(i,j)}, e^{(i',j')} \right\rangle_w = \sum_{\mathcal{A} \in \mathrm{LS}_\epsilon^{(\underline{n})}} w_\mathcal{A} \hat{T}_i(x_\mathcal{A}) \hat{T}_j(y_\mathcal{A}) \hat{T}_{i'}(x_\mathcal{A}) \hat{T}_{j'}(y_\mathcal{A}) = \langle \hat{T}_i(x)\hat{T}_j(y), \hat{T}_{i'}(x)\hat{T}_{j'}(y) \rangle = 0$$

Moreover, if $(i,j) = (i',j')$, Theorem 3.2 implies

$$\left\| e^{(i,j)} \right\|_w^2 = \left\langle e^{(i,j)}, e^{(i,j)} \right\rangle_w = \sum_{\mathcal{A} \in \mathrm{LS}_\epsilon^{(\underline{n})}} w_\mathcal{A} \left(\hat{T}_i(x_\mathcal{A}) \hat{T}_j(y_\mathcal{A}) \right)^2 = \begin{cases} 1 & \text{if } (i,j) \in \Gamma^{(\epsilon\underline{n})} \setminus (0, \epsilon n_2), \\ 2 & \text{if } (i,j) = (0, \epsilon n_2). \end{cases} \tag{19}$$

Therefore, since $\#\mathrm{LS}_\epsilon^{(\underline{n})} = \#\Gamma^{(\epsilon\underline{n})}$, the set $\left\{ e^{(i,j)} : \quad (i,j) \in \Gamma^{(\epsilon\underline{n})} \right\}$ is an orthogonal basis of the vector space $\mathbb{R}^{\mathrm{LS}_\epsilon^{(\underline{n})}}$ with respect to the discrete inner product $\langle \cdot, \cdot \rangle_w$. For all $\mathcal{A}, \mathcal{A}' \in \Gamma^{(\epsilon\underline{n})}$, we have

$$L_{\mathcal{A}'}(\mathcal{A}) = w_{\mathcal{A}'} \sum_{(i,j) \in \Gamma^{(\epsilon\underline{n})}} \frac{1}{\| e^{(i,j)} \|_w^2} e^{(i,j)}(\mathcal{A}') \, e^{(i,j)}(\mathcal{A}).$$

Then, for all $(i,j) \in \Gamma^{(\epsilon \underline{n})}$, we can conclude

$$\left\langle L_{\mathcal{A}'}, e^{(i,j)} \right\rangle_w = w_{\mathcal{A}'}\, e^{(i,j)}(\mathcal{A}') = \left\langle \delta_{\mathcal{A}'}, e^{(i,j)} \right\rangle_w,$$

where $\delta_{\mathcal{A}'}$ denotes the Dirac delta function on $\mathrm{LS}_\epsilon^{(\underline{n})}$ corresponding to $\mathcal{A}'$, i.e. $\delta_{\mathcal{A}'}(\mathcal{A}) = 1$ if $\mathcal{A} = \mathcal{A}'$ and zero otherwise. Therefore, since the functions $e^{(i,j)}$, $(i,j) \in \Gamma^{(\epsilon \underline{n})}$, form a basis of $\mathbb{R}^{\mathrm{LS}_\epsilon^{(\underline{n})}}$, we have $L_{\mathcal{A}'}(\mathcal{A}) = \delta_{\mathcal{A}'}(\mathcal{A})$ for all $\mathcal{A}', \mathcal{A} \in \mathrm{LS}_\epsilon^{(\underline{n})}$. This implies (16). The vector space homomorphism $f \to \mathcal{L}_\epsilon^{(\underline{n})} f(x,y)$ from $\mathbb{R}^{\mathrm{LS}_\epsilon^{(\underline{n})}}$ to $\Pi^{(\epsilon \underline{n})}$ is injective. Since $\dim \mathbb{R}^{\mathrm{LS}_\epsilon^{(\underline{n})}} = \dim \Pi^{(\epsilon \underline{n})}$, this homomorphism is bijective onto $\Pi^{(\epsilon \underline{n})}$. Therefore, $\mathcal{L}_\epsilon^{(\underline{n})} f \in \Pi^{(\epsilon \underline{n})}$ is uniquely determined by (16).

Finally, the definition (17) of $L_{\mathcal{A}}(x,y)$ immediately implies $\mathcal{L}_\epsilon^{(\underline{n})} f(x,y) = \sum_{(i,j) \in \Gamma^{(\epsilon \underline{n})}} c_{ij} \hat{T}_i(x) \hat{T}_j(y)$ for the values in (18). □

According to the just shown proof of Theorem 4.1, the polynomials $L_{\mathcal{A}}$, $\mathcal{A} \in \mathrm{LS}_\epsilon^{(\underline{n})}$, form a basis of the polynomial space $\Pi^{(\epsilon \underline{n})}$ and satisfy $L_{\mathcal{A}'}(\mathcal{A}) = \delta_{\mathcal{A}'}(\mathcal{A})$ for all $\mathcal{A}, \mathcal{A}' \in \mathrm{LS}_\epsilon^{(\underline{n})}$. They are referred to as fundamental polynomials of Lagrange interpolation with respect to the node set $\mathrm{LS}_\epsilon^{(\underline{n})}$.

Remark 3. There exist other ways to prove the interpolation result of Theorem 4.1. For the Padua points, the uniqueness of polynomial interpolation can be proved very elegantly by using ideal theory (cf. [5]). In [15, 16], Theorem 4.1 was proven by using an isomorphism from the polynomial space $\Pi^{(\epsilon \underline{n})}$ into a particular space of trigonometric polynomials on the curve $\boldsymbol{\gamma}_\epsilon^{(\underline{n})}$. In this way, the interpolation problem (16) was reduced to an interpolation problem for trigonometric polynomials.

5 Numerical condition and convergence of polynomial interpolation on Lissajous nodes

For the Padua points and the Xu points it is well-known that the absolute condition number of the interpolation problem grows square logarithmically in the number of node points [3, 4, 13]. A similar behavior of the so called Lebesgue constant can be observed also for the Lissajous node points $\mathrm{LS}_\epsilon^{(\underline{n})}$ [15, 16].

In this section, we summarize some results concerning the growth of the Lebesgue constant and the convergence of the interpolating polynomial $\mathcal{L}_\epsilon^{(\underline{n})} f$ to a given function $f \in C([-1,1]^2)$ if the parameters n_1 and n_2 get large. The original proofs of the convergence results for the Xu and the Padua points can be found in [39] and [5, 10], respectively. The adaption of these proofs to the case of Lissajous node points is elaborated in [15].

As a first type of convergence, we consider mean convergence of the Lagrange interpolation in the L^r-norms

$$\|f\|_r^r := \frac{1}{\pi^2} \int_{-1}^{1} \int_{-1}^{1} |f(x,y)|^r \omega(x,y) \mathrm{d}x\mathrm{d}y, \quad 1 \le r < \infty.$$

The proof of the respective convergence result in Theorem 5.2 is based on the following Marcinkiewicz-Zygmund type inequality (the details can be found in [15]):

Lemma 5.1. *For $1 < r < \infty$, the inequality*

$$D_{r,\epsilon} \|P\|_r^r \le \sum_{\mathcal{A} \in \mathrm{LS}_\epsilon^{(\underline{n})}} w_{\mathcal{A}} |P(\mathcal{A})|^r \le C_{r,\epsilon} \|P\|_r^r \tag{20}$$

holds for all polynomials $P \in \Pi^{(\epsilon \underline{n})}$ with positive constants $C_{r,\epsilon}$ and $D_{r,\epsilon}$ independent of $\underline{\boldsymbol{n}}$. The second inequality in (20) holds also for $r = 1$ with a positive constant $C_{1,\epsilon}$ independent of $\underline{\boldsymbol{n}}$.

Theorem 5.2. *Let $1 \le r < \infty$ and $f \in C([-1,1]^2)$. Further, let $n_{1,k}$ and $n_{2,k}$, $k \in \mathbb{N}$, be sequences of diverging relatively prime natural numbers. Then, the interpolation polynomials $\mathcal{L}_\epsilon^{(\underline{n}_k)} f$ satisfying $\mathcal{L}_\epsilon^{(\underline{n}_k)} f(\mathcal{A}) = f(\mathcal{A})$ for all $\mathcal{A} \in \mathrm{LS}_\epsilon^{\underline{n}_k}$ converge to f in the L^r-norm, i.e.*

$$\lim_{k \to \infty} \|\mathcal{L}_\epsilon^{(\underline{n}_k)} f - f\|_r = 0.$$

Proof. Having the Marcinkievicz-Zygmund inequality (20) at hand, the actual proof is very short and based on a general argumentation scheme described in [29]. If we use the first part of inequality (20) for the polynomial $\mathcal{L}_\epsilon^{(\underline{n}_k)} f \in \Pi^{(\epsilon \underline{n})}$, we get

$$\|\mathcal{L}_\epsilon^{(\underline{n}_k)} f\|_r^r \le D_{r,\epsilon}^{-1} \sum_{\mathcal{A} \in \Gamma^{(\epsilon \underline{n}_k)}} w_{\mathcal{A}} |f(\mathcal{A})|^r \le D_{r,\epsilon}^{-1} \|f\|_\infty^r, \quad 1 < r < \infty.$$

Now, for an arbitrary polynomial $P \in \Pi^N$ with $\Pi^N \subset \Pi^{(\epsilon \underline{n}_k)}$, we have the identity $\mathcal{L}_\epsilon^{(\underline{n}_k)} P = P$ and therefore

$$\|\mathcal{L}_\epsilon^{(\underline{n}_k)} f - f\|_r \le \|\mathcal{L}_\epsilon^{(\underline{n}_k)} (f - P)\|_r + \|P - f\|_r \le (1 + D_{r,\epsilon}^{-1}) \|P - f\|_\infty.$$

Since n_1 and n_2 diverge and the polynomials are dense in $C([-1,1]^2)$, we immediately get mean convergence of the Lagrange interpolant for $1 < r < \infty$. The convergence for $r = 1$ follows analogously using the estimate

$$\|\mathcal{L}_\epsilon^{(\underline{n}_k)} f\|_1 \le \|\mathcal{L}_\epsilon^{(\underline{n}_k)} f\|_2 \le D_{r,\epsilon}^{-1/2} \|f\|_\infty.$$

□

We consider now the absolute condition number of the interpolation problem (16). Using the uniform norm for continuous functions on $[-1,1]^2$, this condition number is explicitly given as the Lebesgue constant

$$\Lambda_\epsilon^{(\underline{n})} := \max_{(x,y)\in[-1,1]^2} \sum_{\mathcal{A}\in \mathrm{LS}_\epsilon^{(\underline{n})}} |L_{\mathcal{A}}(x,y)|.$$

For the Lebesgue constant $\Lambda_\epsilon^{(\underline{n})}$, we have the following estimate. The proof is also partly based on the Marcinkievicz-Zygmund inequality (20). For the details, we refer to [15].

Theorem 5.3. *Let $n_{\min} = \min\{n_1, n_2\}$ and $n_{\max} = \max\{n_1, n_2\}$. The Lebesgue constant $\Lambda_\epsilon^{(\underline{n})}$ is bounded by*

$$D_{\Lambda,\epsilon} \ln^2(n_{\min}) \le \Lambda_\epsilon^{(\underline{n})} \le C_{\Lambda,\epsilon} \ln^2(n_{\max}).$$

The positive constants $C_{\Lambda,\epsilon}$ and $D_{\Lambda,\epsilon}$ do not depend on n_1 and n_2.

The Lebesgue constant is not only important in terms of numerical stability. It is also a crucial factor in the description of the uniform error of the polynomial interpolation. An almost direct consequence of Theorem 5.3 and Jackson's inequality are the following estimates.

Corollary 5.4. *For any continuous function $f \in C([-1,1]^2)$, we have*

$$\|f - \mathcal{L}_\epsilon^{(\underline{n})} f\|_\infty \le (C_{\Lambda,\epsilon} \ln^2(n_{\max}) + 2) E_{n_{\min}}(f),$$

where $E_{n_{\min}}(f)$ denotes the best approximation of f in the polynomial space $\Pi^{n_{\min}}$. In particular, if $f \in C^s([-1,1]^2)$ is s times continuously differentiable and ω_f^s denotes the modulus of continuity of $f^{(s)}$, we have the convergence rate

$$\|f - \mathcal{L}_\epsilon^{(\underline{n})} f\|_\infty \le C \frac{\ln^2(n_{\max})}{n_{\min}^s} \omega_f^s\left(\frac{1}{n_{\min}}\right), \tag{21}$$

with a positive constant C independent of n_1 and n_2.

Considering (21) for $s = 0$, it is possible to introduce a Dini-Lipschitz type condition for continuous functions f such that the right hand side of (21) converges to zero. This condition gets more explicit in the case of Padua and Xu points. For these point sets, it is possible to obtain explicit upper bounds for the Lebesgue constant, cf. [3, 4].

6 Fast computation of the coefficients of the interpolating polynomial

Using the characterization (11) of the points $\mathrm{LS}_\epsilon^{(\underline{n})}$ in terms of Chebyshev-Gauß-Lobatto points, we can derive a fast and efficient scheme for the computation of the coefficients c_{ij} in (18). The single steps of the derivation are almost identical to a respective algorithm developed in [8, 10] for the Padua points.

In a first step, we store all relevant information in different data matrices. The coefficients c_{ij} are collected in the matrix $\mathbf{C}^{(\epsilon\underline{n})} = (c_{ij}) \in \mathbb{R}^{(\epsilon n_1+1)\times(\epsilon n_2+1)}$ as

$$c_{ij} = \begin{cases} \langle \mathcal{L}_\epsilon^{(\underline{n})} f, \hat{T}_i(x)\hat{T}_j(y)\rangle, & \text{if } (i,j) \in \Gamma^{(\epsilon\underline{n})}, \\ 0, & \text{otherwise,} \end{cases}$$

with the indices i, j in the range $i \in \{0,\dots,\epsilon n_1\}$ and $j \in \{0,\dots,\epsilon n_2\}$. The data values $f(\mathcal{A})$ together with the weights $w_{\mathcal{A}}$ are stored in an extended data matrix $\mathbf{G}_f = (g_{ij}) \in \mathbb{R}^{(\epsilon n_1+1)\times(\epsilon n_2+1)}$ with the entries

$$g_{ij} := \begin{cases} w_{\mathcal{A}} f(\mathcal{A}), & \text{if } (z_i^{\epsilon n_1}, z_j^{\epsilon n_2}) \in \mathrm{LS}_\epsilon^{(\underline{n})},\ \mathcal{A} = (z_i^{\epsilon n_1}, z_j^{\epsilon n_2}), \\ 0 & \text{if } (z_i^{\epsilon n_1}, z_j^{\epsilon n_2}) \notin \mathrm{LS}_\epsilon^{(\underline{n})}. \end{cases}$$

Further, for a general finite set $\mathcal{X} = \{x_0,\dots,x_m\} \subset [-1,1]$ of points, we define the matrices

$$\mathbf{T}_n(\mathcal{X}) := \begin{pmatrix} \hat{T}_0(x_0) & \cdots & \hat{T}_0(x_m) \\ \vdots & \ddots & \vdots \\ \hat{T}_n(x_0) & \cdots & \hat{T}_n(x_m) \end{pmatrix} \in \mathbb{R}^{(n+1)\times(m+1)}.$$

Finally, we define a mask $\mathbf{M}^{\epsilon\underline{n}} = (m_{ij}) \in \mathbb{R}^{(\epsilon n_1+1)\times(\epsilon n_2+1)}$ for the index set $\Gamma^{(\epsilon\underline{n})}$ using the entries

$$m_{ij} := \begin{cases} 1, & \text{if } (i,j) \in \Gamma^{(\epsilon\underline{n})} \setminus (0,\epsilon n_2), \\ 1/2, & \text{if } (i,j) = (0,\epsilon n_2), \\ 0, & \text{if } (i,j) \notin \Gamma^{(\epsilon\underline{n})}. \end{cases}$$

Then, in view of (18), the coefficient matrix $\mathbf{C}^{(\epsilon\underline{n})}$ of the interpolating polynomial $\mathcal{L}_\epsilon^{(\underline{n})} f$ can be computed as

$$\mathbf{C}^{(\epsilon\underline{n})} = \left(\mathbf{T}_{\epsilon n_1}(\mathcal{Z}_{\epsilon n_1}) \mathbf{G}_f \mathbf{T}_{\epsilon n_2}(\mathcal{Z}_{\epsilon n_2})^T\right) \odot \mathbf{M}^{(\epsilon\underline{n})}, \tag{22}$$

where $\odot$ denotes pointwise multiplication of the matrix entries and $\mathcal{Z}_{\epsilon n_1} = \{z_0^{\epsilon n_1}, z_1^{\epsilon n_1}, \dots, z_{\epsilon n_1}^{\epsilon n_1}\}$ denotes the set of all Chebyshev-Gauß-Lobatto points. For an arbitrary point $(x,y) \in [-1,1]^2$, the evaluation $\mathcal{L}_\epsilon^{(\underline{n})} f(x,y)$ of the interpolation polynomial is then given by

$$\mathcal{L}_\epsilon^{(\underline{n})} f(x,y) = \mathbf{T}_{\epsilon n_1}(x)^T \mathbf{C}^{(\epsilon \underline{n})} \mathbf{T}_{\epsilon n_2}(y). \tag{23}$$

The matrices $\mathbf{T}_{\epsilon n_1}(\mathcal{Z}_{\epsilon n_1})$ and $\mathbf{T}_{\epsilon n_2}(\mathcal{Z}_{\epsilon n_2})$ have a very particular structure and describe discrete cosine transforms. This makes it possible to evaluate the matrix-matrix products in (22) efficiently using fast Fourier methods. To see the details, we evaluate the matrix products in equation (22) and obtain for the single entries c_{ij} of the matrix $\mathbf{C}^{(\epsilon \underline{n})}$ the formula

$$c_{ij} = m_{ij}\alpha_{ij} \sum_{l=0}^{\epsilon n_2} \left(\sum_{k=0}^{\epsilon n_1} g_{kl} \cos \frac{ik\pi}{\epsilon n_1} \right) \cos \frac{jl\pi}{\epsilon n_2} \tag{24}$$

with the normalization factors α_{ij} defined by $\alpha_{ij} := \sqrt{2-\delta_{0,i}}\sqrt{2-\delta_{0,j}}$. Therefore, the computation of the coefficients c_{ij} can be performed by a composition of two one-dimensional discrete cosine transforms along the columns and the rows of the matrices $\mathbf{G}_f$ and $\mathbf{T}_{\epsilon n_1}(\mathcal{Z}_{\epsilon n_1})\mathbf{G}_f$, respectively. Since

$$\sum_{k=0}^{\epsilon n_1} g_{kl} \cos \frac{ik\pi}{\epsilon n_1} = \operatorname{Re}\left(\sum_{k=0}^{\epsilon n_1} g_{kl}\, e^{-\imath \frac{2\pi i k}{2\epsilon n_1}} \right), \quad l = 0, \dots, \epsilon n_2,$$

the single discrete cosine transforms can be executed efficiently by using a fast Fourier transform for vectors of the form $(g_{0,l}, \cdots, g_{\epsilon n_1, l}, 0, \cdots, 0)^T \in \mathbb{R}^{2\epsilon n_1}$. In a second step, the same procedure can be applied for the discrete cosine transform of the rows of the matrix $\mathbf{T}_{\epsilon n_1}(\mathcal{Z}_{\epsilon n_1})\mathbf{G}_f$. The complexity of the whole algorithm is determined by the complexity of the fast Fourier transforms and is of order $\mathcal{O}(n_1 n_2 \ln(n_1 n_2))$. For the case $\epsilon = 2$, the implementation of formula (24) in Matlab/Octave code can be found in [16].

Remark 4. The matrix formulations in (22) and (23) are direct generalizations of respective matrix equation given for the Padua points in [8, 10]. Also, the efficient computation of the coefficients $\mathbf{C}^{\epsilon \underline{n}}$ based on the fast Fourier transform is an idea developed in [8] for the Padua points. It is not surprising that the same ideas work also in the more general Lissajous case. This is due to the strong similarity in the representation (17) of the Lagrange polynomials as well as in the formula (18) for the coefficients. The main difference to the original scheme of the Padua points is given by the form of the mask matrix $\mathbf{M}^{(\epsilon \underline{n})}$. Whereas in the general Lissajous case the mask $\mathbf{M}^{(\epsilon \underline{n})}$ has an asymmetric structure determined by the index set $\Gamma^{(\epsilon \underline{n})}$, it is an upper left triangular matrix for the Padua points. Two examples of the structure of the index set $\Gamma^{(\epsilon \underline{n})}$ are given in Figure 3.

7 A possible application in Magnetic Particle Imaging

Magnetic Particle Imaging (MPI) is a novel medical imaging technique [21], which is currently available for pre-clinical applications [7] and under development for human applications [2]. The basic concept is to visualize a pre-administered tracer by using several superimposed magnetic fields. MPI promises a high temporal and spatial resolution as well as a very good sensitivity [37]. Further, the tracer material is iron-based and therefore non-hazardous for potential patients. In order to get an idea about current directions and future developments in MPI, an overview can be found, for example, in [31].

The imaging physics of MPI is based on the non-linear magnetization response of the tracer material that consist of superparamagnetic iron-oxide nanoparticles (SPIONs). To this end, an oscillating magnetic field, referred to as a drive field, is applied to excite the SPIONs. As a result, the SPIONs experience a magnetization change that can be measured and reconstructed to an image. In order to achieve a spatial encoding, an additional gradient field, referred to as a selection field, is applied. The combination of drive field and selection field generates a field free point (FFP) that moves along a trajectory in a field of view (FOV). In MPI, typical trajectories used in order to encode a rectangular FOV are Lissajous trajectories [26, 38].

In order to encode a three-dimensional rectangular volume, a promising approach is the generation of a two-dimensional Lissajous curve in the xy-plane that moves with a velocity v_z in the direction of the z-axis [25]. The corresponding elongated Lissajous curve is given as

$$\Upsilon_{\text{elong}}^{(\underline{n})} : \mathbb{R} \to [-b,b]^2 \times \mathbb{R}, \quad \Upsilon_{\text{elong}}^{(\underline{n})}(t) = \begin{pmatrix} b \sin\left(\frac{2\pi n_2}{T} t\right) \\ b \sin\left(\frac{2\pi n_1}{T} t\right) \\ v_z t \end{pmatrix} = \begin{pmatrix} b\, \Upsilon_{\underline{n},\underline{1}}^{(\underline{n})}\left(\frac{2\pi}{T} t\right) \\ v_z t \end{pmatrix},$$

where T denotes the period length and $[-b,b]^2$ the FOV of the Lissajous curve in the xy-plane. An example illustration of a non-elongated and an elongated Lissajous curve is shown in Figure 4. In such a scenario, it is desirable to achieve a maximal elongation with minimal signal loss or distortion artifacts. However, in order to resolve particle signals in z-direction, the velocity v_z should not be chosen too large. A theoretical upper limit for the velocity is given by $v_z = \frac{2X_s}{GT}$, where G is the gradient strength of the selection field and X_s is the range in which SPIONs change their magnetization significantly (see [20, 25]). The node points $\mathrm{LS}_2^{(\underline{n})}$ of the non-degenerate Lissajous curve $\Upsilon_{\underline{n},\underline{1}}^{(\underline{n})}$ can be used to obtain more precise temporal distance maps for points on the sampling path.

In [25], the interior Lissajous node points $\mathrm{LS}_{\text{int},2}^{(\underline{n})}$, i.e. the self-intersection points of the non-degenerate curve $\Upsilon_{\underline{n},\underline{1}}^{(\underline{n})}$, are used to determine temporal differences between corresponding node points within a defined period length T of the trajectory. If t and t' denote two time samples that describe the same self-intersection point $\mathcal{A} = \Upsilon_{\underline{n},\underline{1}}^{(\underline{n})}(\frac{2\pi t}{T}) = \Upsilon_{\underline{n},\underline{1}}^{(\underline{n})}(\frac{2\pi t'}{T}) \in \mathrm{LS}_{\text{int},2}^{(\underline{n})}$, the temporal distance

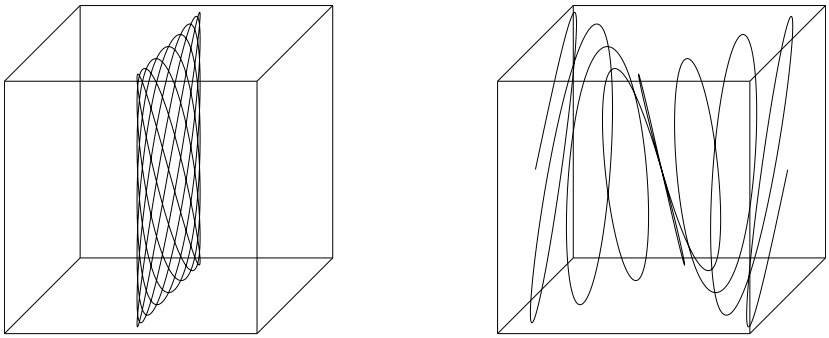

(a) Non-elongated Lissajous curve $\Upsilon^{(8,7)}_{(8,7),\underline{1}}$. (b) Elongated Lissajous curve $\Upsilon^{(8,7)}_{\text{elong}}$.

Figure 4: Example illustration of the Lissajous curve $\Upsilon^{(8,7)}_{(8,7),\underline{1}}$ in non-elongated and elongated form.

between two consecutive crossings of $\mathcal{A}$ is given by $|t-t'|$ or $T-|t-t'|$. Therefore, normalized maximal and minimal temporal distances are given by $\Delta t_{\max}(\mathcal{A}) = \max\{|t-t'|/T, 1-|t-t'|/T\}$ and $\Delta t_{\min}(\mathcal{A}) = \min\{|t-t'|/T, 1-|t-t'|/T\}$, respectively.

An example illustration of $\Delta t_{\max}$ for the node points $\mathrm{LS}_2^{(8,7)}$ is shown in Figure 5. In addition to the specific temporal differences at the node points $\mathrm{LS}_2^{(8,7)}$, interpolated difference maps are given. We use linear interpolation and the polynomial Lagrange interpolation derived in Theorem 4.1 as interpolation methods. It can be seen that the interpolating polynomial shows some over- and undershoot between the node points, whereas, as expected, the linear interpolation avoids this problem.

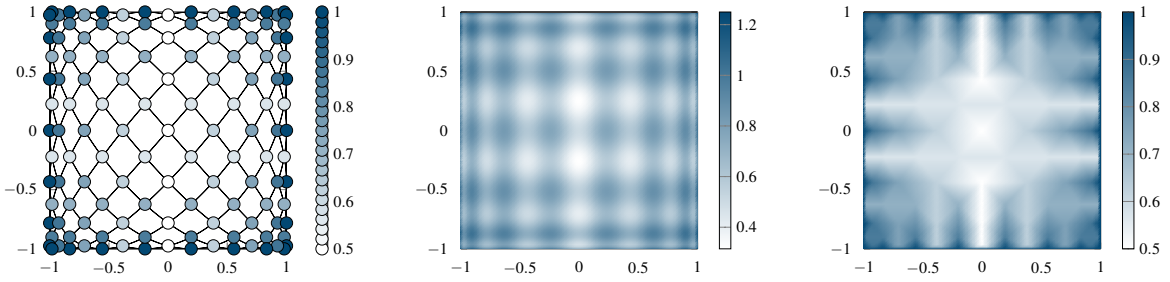

(a) $\mathrm{LS}_2^{(8,7)}$ with $\Delta t_{\max}$. (b) Lagrange interpolation. (c) Linear interpolation.

Figure 5: Illustration of the maximal temporal differences for the node points $\mathrm{LS}_2^{(8,7)}$ of the Lissajous curve as well as the respective interpolated difference maps. The chosen interpolation techniques are a linear and a Lagrange interpolation.

As a further application example, we compare an MPI simulation based on an elongated Lissajous trajectory $\Upsilon^{(32,31)}_{\text{elong}}$ with a simulation based on a non-elongated one. Ideal magnetic fields are used to generate the particle signal, whereas the gradient strength is $G = 2\,\mathrm{T m^{-1}}\mu_0^{-1}$ in y direction and $1\,\mathrm{T m^{-1}}\mu_0^{-1}$ in x and z directions (μ_0 denotes the vacuum permeability). The elongation of the Lissajous trajectory in axial direction is simulated by the application of an additional linear focus field [21, 35]. The FOV size is chosen to be $1\,\mathrm{cm} \times 1\,\mathrm{cm} \times 4X_S G^{-1}$ discretized into $101 \times 101 \times 3$ voxels. The noise model is chosen in accordance with [37]. The simulated MPI tracer that is used for this phantom is based on the Langevin theory assuming undiluted Resovist® (Bayer Schering Pharma AG, Berlin, Germany) with particles of a size of 30 nm and $X_S = 1.1\,\mathrm{mT}\mu_0^{-1}$ [20].

For both, the non-elongated and the elongated case, the imaging plane is located in the xy-plane and is positioned at $z = 2X_S G^{-1}$ in the center of the field of view. In the non-elongated case the Lissajous trajectory fully covers the imaging plane. For the elongated case, the velocity is chosen as $v_z = 2X_S G^{-1} T^{-1}$ such that at $t = T$ the imaging plane is reached. The reconstruction is performed based on a predetermined system matrix and an iterative Kaczmarz approach with additional Tikhonov regularization [22]. The results of the simulations are shown in Figure 6.

The reconstruction of the circular structures, when the Lissajous trajectory is not elongated, appears to be as expected with a good signal intensity and no major distortions. For the elongated case, it can be seen that the reconstructed signal intensities are comparable to the non-elongated case and that the circular structures are more distorted towards the main diagonal than the structures towards the top left and the bottom right corner of the image. A possible explanation of this phenomenon can be given by the incorporation of the maximal distances of the node points $\mathrm{LS}_2^{(\underline{n})}$ to the chosen position z of the imaging plane.

In Figure 7, the normalized maximal distances

$$\Delta z_{\max}(\mathcal{A}) = \max\left\{ \frac{|z - v_z t|}{z} : \quad t \in \left[\tfrac{T}{2}, \tfrac{3T}{2}\right], \quad \Upsilon^{(\underline{n})}_{\underline{n},\underline{1}}\left(\tfrac{2\pi t}{T}\right) = \mathcal{A} \right\}$$

to the imaging plane at $z = 2X_S G^{-1}$ are shown for each of the node points. It should be noted that in this case the order $\underline{n} = (8,7)$

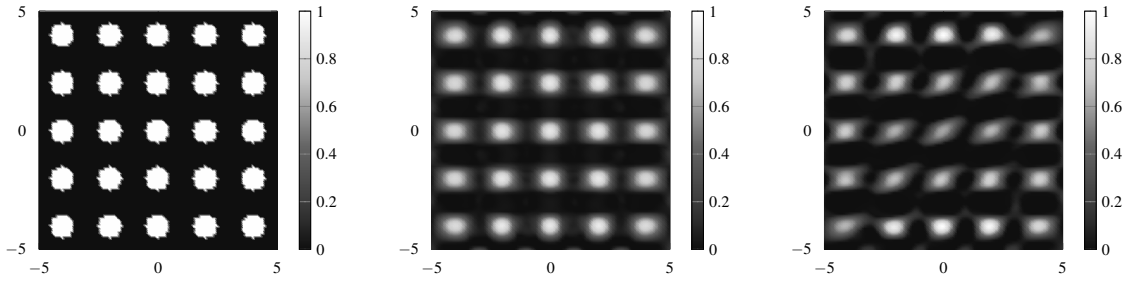

(a) Phantom. (b) Reconstruction based on $\Upsilon^{(32,31)}_{(32,31),\underline{\mathbf{1}}}$. (c) Reconstruction based on $\Upsilon^{(32,31)}_{\text{elong}}$.

Figure 6: Visualization of the chosen phantom and the reconstruction results based on a non-elongated and an elongated Lissajous trajectory with velocity $v_z = 2X_S G^{-1} T^{-1}$. The reconstructed values are normalized in the range $[0, 1]$. The dimensions are given in mm.

of the node points $\mathrm{LS}_2^{(8,7)}$ is chosen for a better illustration of the results and that the statement holds for higher orders $\underline{\boldsymbol{n}}$ as well. Furthermore, the maximal distances are presented in form of interpolated distance maps that are based on a linear and a Lagrange interpolation. As already observed in the reconstructed image of the elongated case, the distances from the node points to the imaging plane increase from the top left and the top right corner towards the main diagonal. This means that there could be a direct relation to the occurrence of the distortion artifacts seen in Figure 6 (c) and the maximal distance $\Delta z_{\max}$ of the node points $\mathrm{LS}_2^{(8,7)}$ to the respective imaging plane.

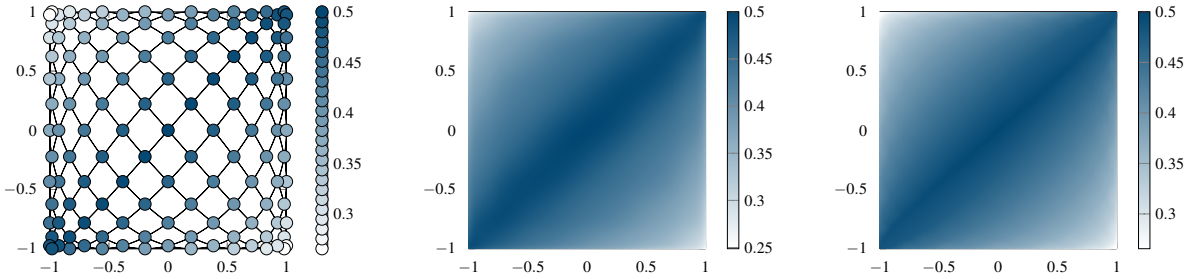

(a) $\mathrm{LS}_2^{(8,7)}$ with maximal distance $\Delta z_{\max}$ to the imaging plane $z = 2X_S G^{-1}$. (b) Lagrange interpolation. (c) Linear interpolation.

Figure 7: Illustration of the maximal distances $\Delta z_{\max}$ of the node points $\mathrm{LS}_2^{(8,7)}$ to an imaging plane in the xy-plane at $z = 2X_S G^{-1}$. In addition to the distances at the node points, interpolated distance maps are given. The interpolation methods are a linear and a polynomial Lagrange interpolation.

Acknowledgements

The authors gratefully acknowledge the financial support of the German Research Foundation (DFG, grant number ER 777/1-1).

References

[1] Bogle, M. G. V., Hearst, J. E., Jones, V. F. R., and Stoilov, L. Lissajous knots. *J. Knot Theory Ramifications 3*, 2 (1994), 121–140.

[2] Borgert, J., Schmidt, J. D., Schmale, I., Bontus, C., Gleich, B., David, B., Weizenecker, J., Jockram, J., Lauruschkat, C., Mende, O., Heinrich, M., Halkola, A., Bergmann, J., Woywode, O., and Rahmer, J. Perspectives on clinical magnetic particle imaging. *Biomedizinische Technik/Biomedical Engineering 58*, 6 (2013), 551 – 556.

[3] Bos, L., Caliari, M., De Marchi, S., Vianello, M., and Xu, Y. Bivariate Lagrange interpolation at the Padua points: the generating curve approach. *J. Approx. Theory 143*, 1 (2006), 15–25.

[4] Bos, L., De Marchi, S., and Vianello, M. On the Lebesgue constant for the Xu interpolation formula. *J. Approx. Theory 141*, 2 (2006), 134–141.

[5] Bos, L., De Marchi, S., Vianello, M., and Xu, Y. Bivariate Lagrange interpolation at the Padua points: the ideal theory approach. *Numer. Math. 108*, 1 (2007), 43–57.

[6] Braun, W. *Die Singularitäten der Lissajous'schen Stimmgabelcurven: Inaugural-Dissertation der philosophischen Facultät zu Erlangen*. Dissertation, Erlangen, 1875.

[7] Bruker Biospin MRI GmbH, Ettlingen, Germany. MPI PreClinical Brochure. https://www.bruker.com/fileadmin/user_upload/8-PDF-Docs/PreclinicalImaging/Brochures/MPI-PreClinical-Brochure.pdf, accessed 26 August 2015.

[8] Caliari, M., De Marchi, S., Sommariva, A., and Vianello, M. Padua2DM: fast interpolation and cubature at the Padua points in Matlab/Octave. *Numer. Algorithms 56*, 1 (2011), 45–60.

[9] Caliari, M., De Marchi, S., and Vianello, M. Bivariate polynomial interpolation on the square at new nodal sets. *Appl. Math. Comput. 165*, 2 (2005), 261–274.

[10] Caliari, M., De Marchi, S., and Vianello, M. Bivariate Lagrange interpolation at the Padua points: Computational aspects. *J. Comput. Appl. Math. 221*, 2 (2008), 284–292.

[11] Cools, R. Constructing cubature formulae: the science behind the art. *Acta Numerica 6* (1997), 1–54.

[12] Cools, R., and Poppe, K. Chebyshev lattices, a unifying framework for cubature with Chebyshev weight function. *BIT 51*, 2 (2011), 275–288.

[13] Della Vecchia, B., Mastroianni, G., and Vértesi, P. Exact order of the Lebesgue constants for bivariate Lagrange interpolation at certain node-systems. *Stud. Sci. Math. Hung. 46*, 1 (2009), 97–102.

[14] Dunkl, C. F., and Xu, Y. *Orthogonal Polynomials of Several Variables*. Cambridge University Press, Cambridge, 2001.

[15] Erb, W. Bivariate Lagrange interpolation at the node points of Lissajous curves - the degenerate case. *arXiv:1503.00895 [math.NA]* (2015).

[16] Erb, W., Kaethner, C., Ahlborg, M., and Buzug, T. M. Bivariate Lagrange interpolation at the node points of non-degenerate Lissajous curves. *Numer. Math.* (2015). DOI: 10.1007/s00211-015-0762-1.

[17] Fischer, G. *Plane algebraic curves. Translated by Leslie Kay*. American Mathematical Society (AMS), Providence, RI, 2001.

[18] Gasca, M., and Sauer, T. On the history of multivariate polynomial interpolation. *J. Comput. Appl. Math. 122*, 1-2 (2000), 23–35.

[19] Gasca, M., and Sauer, T. Polynomial interpolation in several variables. *Adv. Comput. Math. 12*, 4 (2000), 377–410.

[20] Gleich, B. *Principles and Applications of Magnetic Particle Imaging*. Springer Vieweg, Wiesbaden, 2014.

[21] Gleich, B., and Weizenecker, J. Tomographic imaging using the nonlinear response of magnetic particles. *Nature 435*, 7046 (2005), 1214–1217.

[22] Grüttner, M., Knopp, T., Franke, J., Heidenreich, M., Rahmer, J., Halkola, A., Kaethner, C., Borgert, J., and Buzug, T. M. On the formulation of the image reconstruction problem in magnetic particle imaging. *Biomedizinische Technik/Biomedical Engineering 58*, 6 (2013), 583–591.

[23] Harris, L. A. Bivariate Lagrange interpolation at the Chebyshev nodes. *Proc. Am. Math. Soc. 138*, 12 (2010), 4447–4453.

[24] Harris, L. A. Bivariate Lagrange interpolation at the Geronimus nodes. *Contemp. Math. 591* (2013), 135–147.

[25] Kaethner, C., Ahlborg, M., Bringout, G., Weber, M., and Buzug, T. M. Axially elongated field-free point data acquisition in magnetic particle imaging. *IEEE Trans. Med. Imag. 34*, 2 (2014), 381–387.

[26] Knopp, T., Biederer, S., Sattel, T. F., Weizenecker, J., Gleich, B., Borgert, J., and Buzug, T. M. Trajectory analysis for magnetic particle imaging. *Phys. Med. Biol. 54*, 2 (2009), 385–3971.

[27] Koseleff, P.-V., and Pecker, D. Chebyshev knots. *J. Knot Theory Ramifications 20*, 4 (2011), 575–593.

[28] Lissajous, J. Mémoire sur l'etude optique des mouvements vibratoires. *Ann. Chim. Phys 51* (1857), 147–231.

[29] Lubinsky, D. Marcinkiewicz-Zygmund inequalities: Methods and results. In *Recent Progress in Inequalities*, G. Milovanović, Ed., vol. 430 of *Mathematics and Its Applications*. Springer Netherlands, 1998, pp. 213–240.

[30] Morrow, C. R., and Patterson, T. N. L. Construction of algebraic cubature rules using polynomial ideal theory. *SIAM J. Numer. Anal. 15* (1978), 953–976.

[31] Panagiotopoulos, N., Duschka, R., Ahlborg, M., Bringout, G., Debbeler, C., Graeser, M., Kaethner, C., Lüdtke-Buzug, K., Medimagh, H., Stelzner, J., Buzug, T., Barkhausen, J., Vogt, F., and Haegele, J. Magnetic particle imaging - current developments and future directions. *International Journal of Nanomedicine 10* (2015), 3097–3114.

[32] Poppe, K., and Cools, R. In search for good chebyshev lattices. In *Monte Carlo and Quasi-Monte Carlo Methods 2010*, L. Plaskota and H. Woźniakowski, Eds., vol. 23 of *Springer Proceedings in Mathematics & Statistics*. Springer Berlin Heidelberg, 2012, pp. 639–654.

[33] Poppe, K., and Cools, R. CHEBINT: a MATLAB/Octave toolbox for fast multivariate integration and interpolation based on Chebyshev approximations over hypercubes. *ACM Trans. Math. Softw. 40*, 1 (2013), 2:1–2:13.

[34] Potts, D., and Volkmer, T. Fast and exact reconstruction of arbitrary multivariate algebraic polynomials in Chebyshev form. In *Proceedings of the 11th International Conference on Sampling Theory and Applications* (2015), pp. 392–396.

[35] Schmale, I., Rahmer, J., Gleich, B., Kanzenbach, J., Schmidt, J. D., Bontus, C., Woywode, O., and Borgert, J. First phantom and in vivo MPI images with an extended field of view. In *Proceedings of SPIE Medical Imaging 2011: Biomedical Applications in Molecular, Structural, and Functional Imaging* (2011), vol. 7965.

[36] Sloan, I. H. Polynomial interpolation and hyperinterpolation over general regions. *J. Approx. Theory 83*, 2 (1995), 238–254.

[37] Weizenecker, J., Borgert, J., and Gleich, B. A simulation study on the resolution and sensitivity of magnetic particle imaging. *Physics in Medicine and Biology 52*, 21 (2007), 6363–6374.

[38] Weizenecker, J., Gleich, B., Rahmer, J., Dahnke, H., and Borgert, J. Three-dimensional real-time in vivo magnetic particle imaging. *Physics in Medicine and Biology 54*, 5 (2009), L1 – L10.

[39] Xu, Y. Lagrange interpolation on Chebyshev points of two variables. *J. Approx. Theory 87*, 2 (1996), 220–238.